ECOLOGICAL SOCIETY OF AMERICA

Ecology/Ecological Monographs/Ecological Applications

PREPRINT

Arranged for: Ecological Applications

Running head: Foliar traits from imaging spectroscopy

Imaging spectroscopy algorithms for mapping canopy foliar chemical and morphological traits and their uncertainties

Aditya Singh[1*], Shawn P. Serbin[1#], Brenden E. McNeil[2], Clayton C. Kingdon[1], Philip A. Townsend[1]

[1]Department of Forest and Wildlife Ecology,
University of Wisconsin-Madison, 1630 Linden Dr. Madison, WI 53706

[2]Department of Geology and Geography,
West Virginia University, Morgantown, WV 26506

***Corresponding Author:**
Aditya Singh
AB13 Russell labs, 1630 Linden Dr,
Madison, WI 53706
Phone: (608) 263-9107
Fax: (608) 262-9922
Email: singh22@wisc.edu

[#]Present address: Shawn P. Serbin, Biological, Environmental & Climate Sciences Department, Brookhaven National Laboratory, Upton, NY 11973-5000. Email: sserbin@bnl.gov

Abstract

A major goal of remote sensing is the development of generalizable algorithms to repeatedly and accurately map ecosystem properties across space and time. Imaging spectroscopy has great potential to map vegetation traits that cannot be retrieved from broadband spectral data, but rarely have such methods been tested across broad regions. Here we illustrate a general approach for estimating key foliar chemical and morphological traits through space and time using NASA's Airborne Visible / Infrared Imaging Spectrometer (AVIRIS-Classic). We apply partial least squares regression (PLSR) to data from 237 field plots within 51 images acquired between2008-2011. Using a series of 500 randomized 50/50 subsets of the original data, we generated spatially explicit maps of seven traits (leaf mass per area [M_{area}], percent nitrogen, carbon, fiber, lignin, cellulose and isotopic nitrogen concentration: $\delta^{15}N$) as well as pixel-wise uncertainties in their estimates based on error propagation in the analytical methods. Both M_{area} and %N PLSR models had a R^2 greater than 0.85. Root mean square errors (RMSEs) for both variables were less than 9% of the range of data. Fiber and lignin were predicted with $R^2 > 0.65$ and carbon and cellulose with $R^2 > 0.45$. Although R^2 of %C and cellulose were lower than M_{area} and %N, the measured variability of these constituents (especially %C) was also lower, and their RMSE values were beneath 12% of the range in overall variability. Model performance for $\delta^{15}N$was the lowest ($R^2 = 0.48$, RMSE =0.95‰) but within 15% of the observed range. The resulting maps of chemical and morphological traits together with their overall uncertainties represent a first-of-its-kind approach for examining the spatio-temporal patterns of forest functioning and nutrient cycling across a broad range of temperate and sub-boreal ecosystems. These results offer an alternative to categorical maps of functional or physiognomic types by providing non-discrete maps (i.e. on a continuum) of traits that define those functional types. A

key contribution of this work is the ability to assign retrieval uncertainties by pixel, a requirement to enable assimilation of these data products into ecosystem modeling frameworks to constrain carbon and nutrient cycling projections.

Key words: imaging spectroscopy, PLS regression, foliar traits, spatial mapping, uncertainty

Introduction

Terrestrial ecosystems play an important role in the global carbon cycle by sequestering 3-5 Pg of carbon (C) per year from the atmosphere via photosynthesis (see Schimel 1995, Cramer et al. 2001, 2007, Le Quere et al. 2009). Characterization of the factors that influence terrestrial C uptake is required to develop an improved process-based understanding of ecosystem dynamics and accurately model vegetation response to global change. However, there remains a large uncertainty in the magnitude, seasonality, and location of this flux (Friedlingstein et al. 2014).

Chemical, structural and morphological properties of the foliage in vegetation canopies correlate strongly with plant function, including ecosystem-wide nutrient cycling rates (Scott and Binkley 1997, Craine et al. 2002, Santiago et al. 2004, Meier and Bowman 2008) and photosynthetic capacity (Reich et al. 1997, Reich et al. 1999, Shipley et al. 2005, Kergoat et al. 2008). Thus, to map ecosystem productivity, modeling efforts to estimate the dynamics of global carbon stocks should make use of "functional biogeographic" (Violle et al. 2014) information on the covariance between plant traits and patterns of biogeochemical cycling (Enquist et al. 2007). The use of remote imaging spectroscopy to map key plant trait patterns — those that govern carbon and nutrient dynamics — will greatly enhance our understanding of ecosystem functioning (Ustin and Gamon 2010).

Global patterns of nutrient cycling and primary productivity in forested ecosystems are driven, in large part, by a tractable suite of foliar structural and biochemical traits representing a tradeoff between leaf construction costs and photosynthetic carbon uptake potential (Reich et al. 1992, Shipley and Lechowicz 2000, Wright et al. 2004, Shipley et al. 2005, Shipley et al. 2006). This defines a spectrum of plant functionfrom slow growing, nutrient poor species to fast growing nutrient rich, albeit "leaky", plants. Specifically, coordination between foliar nitrogen

content and specific leaf area (SLA, or its reciprocal, leaf mass per area, M_{area}) maximizes C-fixation (Shipley et al. 2005), with lower SLA resulting in lower foliage photosynthetic potential per unit dry mass (Niinemets 2001) but greater leaf structural strength and consequently longer leaf life spans (Wright and Westoby 2002, Wright et al. 2005a, Violle et al. 2009). These patterns have been found to be consistent between broadleaf, needleleaf and herbaceous species (Reich et al. 1991, Reich et al. 1992, Grime 2006) and have been found to operate independent of growth form or phylogeny (Shipley et al. 2006). Foliar nitrogen content (i.e. nitrogen on scaled to an area basis, g m^{-2}) scales with the content of RuBisCo, the key protein responsible for the carboxylation of RuBP in the initial steps of CO_2 fixation (Long 1991, Collatz et al. 1992, Ainsworth and Rogers 2007). Thus, foliar nitrogen reflects a plant's investment in photosynthetic enzymes, structure, and light harvesting complexes which modulate photosynthetic parameters such as the maximum rates of carboxylation (V_{cmax}) and electron transport (J_{max}) (Long 1991, Ripullone et al. 2003).

Foliar nitrogen concentration and M_{area}/SLA also co-vary strongly with decomposition and nitrogen mineralization rates across ecosystems (Chapin 2003, Kazakou et al. 2006, Quested et al. 2007, Santiago 2007). Decomposition releases plant nutrients and drives the largest flux of terrestrial C to the atmosphere (Meier and Bowman 2008), and rates of decomposition are positively correlated with nitrogen content of foliage and litter, SLA and leaf water content (Bonan 1993, Hattenschwiler et al. 2005, Fortunel et al. 2009) and negatively with leaf dry matter content (Quested et al. 2007, Fortunel et al. 2009, Kazakou et al. 2009) and foliar lignin concentrations (Hobbie et al. 2007, Johnson et al. 2007, Carrera and Bertiller 2010). Foliar lignin-to-nitrogen ratios are thus strong indicators of litter quality and consistent predictors of litter decomposability (Melillo et al. 1982, Knorr et al. 2005, Fortunel et al. 2009) and, together

with cellulose concentration, regulate rates of late-stage forest litter decomposition (McClaugherty and Berg 1987, Berg 2000, Johnson et al. 2007).

Foliar isotopic N concentration ($\delta^{15}N$) is an integrator of the nitrogen cycle (Robinson 2001, Amundson et al. 2003) and has been used as an indicator of relative N availability to plants and a basis to infer N cycling rates (Austin and Vitousek 1998, Martinelli et al. 1999, Craine et al. 2009). Specifically, variations in N fractionation in foliar matter can indicate effects of climate on organic/inorganic nitrogen availability (Amundson et al. 2003, Craine et al. 2009) or local-scale variations in plant dependence on mycorrhizal associations (Hogberg 1997, Hobbie et al. 2000, Lilleskov et al. 2002, Craine et al. 2009). Spatial patterns of foliar isotopic N concentrations are also associated with plant response to disturbances (Amundson et al. 2003, McLauchlan et al. 2007) or elevated external inputs such as N deposition (Hogberg 1997, Emmett et al. 1998, McLauchlan et al. 2007).

Synoptic, repeatable and consistent retrievals of key foliar traits such as foliar nitrogen, SLA (or M_{area}), foliar lignin and cellulose and isotopic nitrogen are invaluable for characterizing determinants of ecosystem function across large regions (Chapin et al. 1996, Diaz et al. 2004, Ustin and Gamon 2010), and may provide valuable inputs for modeling nutrient fluxes and vegetation range shifts under changing land-use and climate scenarios (Wright et al. 2004, Townsend et al. 2008). Remote sensing – specifically imaging spectroscopy – offers the capacity to map the primary drivers of plant trait variability from the landscape to the global scale (Ustin and Gamon 2010). Imaging spectrometers measure reflected light in narrow, contiguous wavebands (typically ≤10-15 nm) over a large portion of the incident solar spectrum (e.g. 350-2500 nm for NASA's Airborne Visible/Infrared Imaging Spectrometer, AVIRIS, Vane et al. 1993, Green et al. 1998). It has long been demonstrated that reflectance spectroscopy is sensitive

to foliar chemistryas well as the structural / morphological characteristics of plant canopies, and indeed, this is the basis for standard spectroscopic approaches to estimate chemistry on dried samples (Kokaly 2001, Richardson and Reeves 2005, Petisco et al. 2006) as well as to non-destructively estimate chemistry or photosynthetic properties of fresh leaves (Curran et al. 1992, Sims and Gamon 2002, Blackburn 2007, Menesatti et al. 2010). The ability to do this is a consequence of well-known biochemical absorption features at different wavelengths (Curran 1989, Curran et al. 1992, Fourty et al. 1996, Curran et al. 2001) related to electron transitions and bending and stretching of chemical bonds (Curran 1989, Fourty et al. 1996).

The ability to retrieve chemistry from remotely sensed imagery is complicated by a number of factors, including crown architecture and seasonality, although it is clear that chemical features related to leaf chlorophyll (Curran et al. 1992, Yoder and Pettigrewcrosby 1995, Curran et al. 2001) and water content are clearly expressed in both narrowband and broadband imagery (Gates et al. 1965, Tucker 1980, Asner and Vitousek 2005, Sanchez-Azofeifa et al. 2009, Ustin et al. 2012). The effects of canopy structure on reflectance may confound the identification of absorption features in foliage (Knyazikhin et al. 2013), for example in wavelengths with highleaf scattering, but there is also strong evidence that features identifiable at the leaf-level can be detected in measurements at the canopy level (Baret et al. 1994). Ultimately, the coordination of traits at both the leaf and canopy level facilitates using spectral information to map traits of interest, even if the biophysical drivers of strong correlations at some wavelengths have not yet been fully characterized (Townsend et al. 2003, Ollinger 2011, Ollinger et al. 2013).

An extensive body of literature has demonstrated the capacity of imaging spectroscopy to map foliar traits relevant to photosynthesis (Wessman et al. 1989, Matson et al. 1994, Curran et al. 1997, Martin and Aber 1997, Coops et al. 2003, Smith et al. 2003, Townsend et al. 2003,

Asner and Martin 2008, Martin et al. 2008, McNeil et al. 2008, Kokaly et al. 2009). In particular, spectra in the shortwave infrared (especially 1400-1850 nm and 2000-2400 nm) are critical to retrieval of parameters related to photosynthesis on account of strong absorption features related to nitrogen bonds in proteins that are expressed in those regions (Fourty et al. 1996). Studies also show that radiative transfer models (Asner 1998, Asner et al. 2008, Asner and Martin 2008, 2009, Asner et al. 2011a) can be used in conjunction with imaging spectroscopy to effectively map foliar traits. In general, existing efforts have been site-specific (Martin and Aber 1997, Ollinger et al. 2002, Coops et al. 2003, Townsend et al. 2003) and, apart from Martin et al. (2008), studies that incorporate information from multiple scenes across multiple locations are rare (Appendix A, Table A1). Here, we report a set of generalizable spectroscopic calibrations for the determination of leaf chemical composition (nitrogen, carbon, and fiber constituents), morphology (leaf mass per area, M_{area}) and isotopic composition ($\delta^{15}N$) of temperate and boreal tree species using imaging spectroscopy. Moreover, by demonstrating techniques to explicitly propagate uncertainties from the leaf to stand to image level, we show how our algorithms can be directly integrated into global change models that require uncertainty estimates of input parameters.

Materials and methods

Study sites

We established 237 plots across a broad swath of the Upper Midwest and Northeast USA (Figure 1). These plots sampled a range of broad- and needle-leaf forests, including36 dominant species (see Appendix A table A2) reported by Serbin et al. (2014). Each plot consisted of two crossing 60×60 m transects, defining five points at which a metric factor 2 prism was used to tally trees by species (Townsend et al. 2003). Foliar biomass by species was estimated from diameter-

biomass relationships in Jenkins et al. (2003), which was subsequently used to scale foliar trait estimates by species to the canopy of the entire plot.

We collected foliage from the top, middle and bottom of the canopy of the predominant species on each plot (>5% of relative biomass) using a shotgun, line launcher or pole pruner Plot-level values for each trait were estimated from the relative proportion of foliar biomass by species on a plot. We measured leaf-level percent nitrogen (%N), carbon (%C), fiber (ADF), lignin (ADL) and cellulose, as well isotopic 15N:14N ($\delta^{15}N$) and leaf mass per area (M_{area}) and their uncertainties by species and by plot from reflectance spectroscopy on both dry and fresh samples (Serbin et al. 2014). Leaf level trait measurements employed chemometric partial least-squares regression (PLSR) models that link contact reflectance spectra and measurements made using standard laboratory techniques. This approach facilitated estimation of per-sample (i.e. per leaf) uncertainties of trait estimates. We scaled measurement uncertainty from leaf-level traits to estimates of canopy traits based on proportional foliar biomass. Leaf-to-canopy trait scaling used 1000 replicates drawn from the distributions of leaf-level estimates and their uncertainties from Serbin et al. (2014) to generate plot-level trait estimates and uncertainties. Note that we had trait estimates for multiple levels of the canopy at each plot, which facilitated testing the ability to map "whole-canopy" trait characteristics (see Ollinger et al. 2002) vs. top-of-canopy traits (presumably all that is visible to the sensor). Using data from Green et al. (2003) on vertical variation in foliar traits within a canopy profile, plot-level estimates were weighted according to four different schemes: A) top weighted – 90% weight for top-of-canopy foliage, 9% weight for mid-canopy foliage and 1% weight for bottom-canopy foliage; B) top-to-middle weighted – 64.5%, 32.3% and 3.2% weights for top, middle and bottom canopy foliage, C) whole canopy – 40%, 40% and 20% weights for top, middle and bottom canopy foliage and D) top only - where

only the top-of-canopy foliage was considered (100% for top-of-canopy). We report results from top weighted scaling (option A described above), but results and coefficients for the rest of the scaling options are provided in the supplements (Appendix A, supplements 2A-2D). For each of these options, uncertainty in relative foliar biomass was incorporated by randomly varying species-level biomass estimates by ±25% in each of the 1000 permutations. Supplement 1 provides plot locations, plot-level canopy trait estimates and associated uncertainties.

Image Processing

145 AVIRIS-Classic images were acquired from NASA's ER-2 platform during the summers of 2008-2011 at flight altitudes ranging from 14,000-20,000 m (pixel sizes of 12-18 m, Fig. 1). Data were provided by the Jet Propulsion Laboratory as orthorectified, calibrated radiance images (Vane et al. 1993, Green et al. 1998) and all images were processed using a common processing stream to ensure comparability. We atmospherically corrected images using ATREM (TAFKAA algorithm: Gao et al. 2000, Montes and Gao 2004). Images were topographically corrected using the modified sun-canopy-sensor topographic method (Soenen et al. 2005) and BRDF (i.e. cross-track) corrected using a quadratic function of the volumetric scattering term of the Ross-Thick BRDF model (Roujean et al. 1992, Lucht et al. 2000). Post-hoc georectification was performed on a small number of poorly-aligned images, with final pixel registration errors < 0.5 pixel across all scenes. 51 images were used for model development and the remainder for testing and analysis.

Statistical analysis

The general approach to the estimation of canopy traits (including chemistry) from imaging spectroscopy (IS) is illustrated in Fig2. We build upon the approach taken by Martin et al. (2008), in which they used data from 8 study sites and 137 field plots to develop a general, cross-scene predictive equation for foliar nitrogen. We extend their effort by additionally deriving maps of carbon, leaf mass per area (M_{area}), fiber, lignin and cellulose, as well as mapping uncertainties in all traits of interest. For each trait, we developed models using 500 permutations of our data, drawing randomly from the plot-level trait estimates and perturbing those estimates based on uncertainties propagated at every level of measurement (spectra, trait, foliar biomass, etc.). For each of the 500 permutations, we randomly split our data 50/50 for calibration and validation. As spectra for a given plot could have been sourced from multiple images available for each location, we further constrained the selection such that an observation could appear only once in the training set (i.e. training spectra for each plot came from a single image). This procedure was repeated 500 times and model coefficients, model fits and predictions were saved for all iterations. We subsequently applied the 500 models to each pixel in all images. This allowed us to report the range of expected model performance and to calculate pixel-by-pixel uncertainty for the mapped models as the standard deviation of model predictions for all 500 permutations. To test if our models were stable across space and time, we conducted additional cross-validations by reformulating PLSR models by leaving out data from a) individual geographic locations (areas with groups of plots, Fig. 1) or b) years of image acquisition and evaluating model fits on the withheld data.

We employed Partial Least-Squares Regression (PLSR; Wold et al. 1984, Geladi and Kowalski 1986, Wolter et al. 2008) to predict canopy traits from imaging spectroscopy, as done

in many previous studies (Coops et al. 2003, Smith et al. 2003, Townsend et al. 2003, Martin et al. 2008, McNeil et al. 2008, Deel et al. 2012). In practice, PLSR iteratively transforms predictor and response variables to find latent vectors and subsequently produce calibration factors and a linear model. PLS techniques achieve computational efficiency by maximizing the covariance between independent and dependent variables while simultaneously maintaining the constraint of being orthogonal to the previously determined factors (Wold et al. 1984, Geladi and Kowalski 1986, Frank and Friedman 1993, Wold et al. 2001). PLSR is better suited than traditional multiple linear regression methods for handling multi-collinear and over-sampled data, i.e. when the number of independent variables approaches or exceeds the number of observations (Woldetal.1984,GeladiandKowalski1986,Woldetal.2001). In particular, variations of unconstrained linear models (such as stepwise variable selection approaches, see Table A1), violate cardinal assumptions of independent predictors and uncorrelated errors. At best, this results in biased estimates of beta coefficients (Tibshirani 1996) and underestimated errors and *P*-values (Altman & Andersen 1989). Specific to chemometric data, stepwise selection procedures have been shown to perform poorly in calibration experiments (see Grossman et al. 1996) and may not generate results based on known absorption characteristics of materials being examined (Townsend et al. 2003). PLSR avoids difficulties in interpretation of synthetic PCA variables or the potential for modeling spurious relationships using stepwise regression (Grossmanetal.1996). The Predicted REsidual Sum of Squares (PRESS) statistic was used to select the appropriate number of PLS model components (Chen et al. 2004). We used the Variable Importance of Projection (VIP) statistic (Wold 1994), and standardized coefficient, by waveband to evaluate the contribution of each wavelength and associated absorption features to trait predictions. The VIP score reflects each predictor's (i.e. waveband) influence in fitting the

PLSR model. It is based on the predictor's absolute coefficient size and partial-R^2 within the overall PLSR model. Standardized coefficients are employed for graphing to account for scale differences in reflectance between different wavelength regions (i.e. higher reflectance and greater variability in the NIR equate to smaller coefficients, but not necessarily less important coefficients) as well as in the dependent variables (traits).

We averaged the 3x3 image pixel array surrounding each field plot's center, leaving us with one composite AVIRIS spectrum per 60x60 m plot. We postulate that averaging surrounding pixels is desirable because field plots in closed-canopy forests can rarely be identified to a specific pixel.

Finally, maps of the traits and their uncertainties were made for all AVIRIS images as the mean (and standard deviation) of the 500 permutations. Geographic patterns of trait distribution were analyzed with respect to gradients of latitude, precipitation and temperature (derived from PRISM 2004) and nitrogen deposition (from NADP 2014).

Results

Geographic variation in foliar traits

Canopy-averaged ranges of plot-level trait estimates stratified by leaf physiognomy are presented in Table 1 (data on plot level foliar traits by species are in Table A2 and the entire data set is in Supplement1). There was a nearly two-fold difference in M_{area} between needleleaf and broadleaf species ($T = 28.88$, $P<0.0001$), and mass-based nitrogen content of broadleaf species was around 1.5 times that of needleleaf species ($T = 24.15$, $P < 0.0001$). Carbon content, fiber, lignin and cellulose exhibited less variation between needle-leaf and broadleaf species, but all differences were significant ($P< 0.0001$). Deciduous-dominated plots showed slightly higher isotopic N

content than coniferous-dominated plots ($T = 2.32$, $P = 0.02$). Correlation analyses revealed a strong negative relationship between leaf nitrogen and M_{area} ($r = -0.766$, $P<0.0001$) as well as significant negative relationships with other leaf structural compounds (Table2). Leaf nitrogen content decreased with latitude, while M_{area} increased, a reflection of an increasing dominance of needleleaf species in the north. We also found a significant positive correlation between foliar nitrogen and patterns of nitrogen deposition across our sites ($r = 0.392$, $P < 0.0001$). To further explore this relationship, we fit a mixed-effects model to predict foliar nitrogen concentrations while controlling for latitude with Gaussian random effects specified for species (not shown). The model explained 88.7% of the variation in foliar nitrogen, of which 59% was attributed to differences between species alone. The effects of elevated foliar nitrogen concentrations corresponding to the N deposition gradient were apparent ($P < 0.0001$) even after taking into consideration latitudinal gradients and inherent differences between species. Foliar $\delta^{15}N$ concentrations were highly correlated with mean annual temperature and declined with mean annual precipitation (MAT $r = 0.413$; MAP $r = -0.455$, both $P < 0.0001$), we also found evidence of foliar isotopic N enrichment along the N deposition gradient ($r = 0.398$, $P< 0.0001$).

Canopy spectra

Canopy spectra were highly variable (Fig.3) with nearly complete separation (±1 standard deviation) between spectra of all broadleaf and all needle-leaf plots in the NIR (700-1400nm) and the 1400-1900 nm SWIR1regions. Spectra of the two physiognomic types partially overlapped in the visible (400-700nm) and SWIR2 (1900-2400nm) wavelengths. The highest spectral variability (in terms of the coefficient of variation, data not shown) was observed in the visible regions of the spectrum (>23-50%) and was generally constant across the rest of the

spectrum (~22%). Across all plots, needle-leaf dominated plots had around 10% less spectral variability than plots dominated by broadleaf species.

PLSR model results

Results for models built using the four aggregation schemes (Appendix A, Table A3) were highly consistent. We provide model comparisons (Figures A1-A5, Appendix A) and PLSR coefficients from all canopy aggregation schemes and randomized models (supplements 2A, 2B, 2C, and 2D), but focus here on results obtained using the top-weighted scheme. In our results, we show the model predictions from AVIRIS vs. field-based measurements (Fig. 4). Note that we show error bars in both directions: error on the Y-axis is due to uncertainty of trait values from the scaling from leaf level spectra to plot level traits, while uncertainty on the X-axis is due to uncertainty from the image-based PLSR model. To our knowledge, this is the first time both uncertainties in the training data and mapped estimates have been provided. We also show standardized coefficients (Fig. 5), to compare wavebands important for mapping different traits. The shaded uncertainties in the standardized coefficients are based on the 500 permutations of the data used to generate the final maps. Additional diagnostics, such as VIP by wavelength and PRESS statistic by number of PLS coefficients (used to select the number coefficients in the PLS model) are graphed in Fig 6. Supplements 2A-2D list the 500 raw PLS coefficients for the traits reported in this paper. These are the values that should be applied to make maps from new images that have been processed consistent with this study. We also show wavelength regions that correspond to known absorption features (from Curran 1989, Fourty et al. 1996, Curran et al. 2001). The standardized coefficients for mapping all of the traits from AVIRIS Classic (except

isotopic N, which has not previously been studied in depth) align in at least some wavelengths with known absorption features (Fig. 5, dotted bars).

Both M_{area} and %N had model fits with R^2 greater than 0.85, which are comparable to the results reported by Martin et al. (2008, Appendix A, Table A2). Root mean square errors (RMSEs) for both variables were less than 9% of the range of data (Tables3). There was considerable spatial variation in retrieval uncertainties for both traits. High uncertainties (e.g. >2% for Nitrogen or > 10% for M_{area}) typically occurred at forest edges, in regions that were likely disturbed and where the dominant species were not represented in our database (e.g. crops or grasses and forbs in recently disturbed areas.). Fiber and lignin were predicted with $R^2 > 0.60$ and carbon and cellulose $R^2 \sim 0.5$. Although R^2 of fiber and lignin were lower than M_{area} and %N, their RMSE values were within 10% of the range of data. The comparatively lower R^2 values for %C and cellulose are related to the low amount of natural variability in these constituents. Isotopic $\delta^{15}N$ had the worst fit of all models ($R^2 = 0.48$) but the RMSE was within 15% of the range in the data. Cross-validations conducted to test model stability across years and sites were in agreement with overall model results. Averaged across all strata (by year or by geographic area) and traits, more than 90% of held-out samples were predicted within the prediction error bounds of calibration models. In addition, validation errors of prediction (RMSEs) were well within the observed range of modeled traits, i.e. with RMSE values lower than 15% of the range of variation in the trait (and usually with %RMSE < 10%, complete results in Supplement 1).

Mapping and application

We used the PLSR-derived coefficients (Supplement 2A) to generate spatially explicit maps of traits and respective uncertainties. We show a subset from one of the many scenes used in this

study (Green Ridge State Forest, MD, Fig. 7).With these maps we synthesized spatial patterns in foliar traits into images of functional variation using false color composites of key foliar traits such as nitrogen, lignin and leaf mass per area (Appendix A, Figure A6). Such maps illustrate gradients of canopy biochemical and morphological traits that are likely related to species associations and provide greater detail than traditional land cover maps. The trait maps expose patterns of plant investment in foliar nutrients vs. structural compounds across environmental gradients on the landscape. Comparison of trait maps among regions reveals variability in relative abundance of traits inferred from, but not captured by, landcover classifications (Appendix A, Figure A6). Maps of functional traits from a single hyperspectral image can reveal differences in species associations across gradients that are otherwise only apparent in multi-date imagery (Appendix A, Figure A7), and, moreover, can help identify ecosystem-level consequences of disturbance events through changes in functional traits and mapped uncertainty (Appendix A, Figure A8).

Discussion

In this study we confirm the capacity of imaging spectroscopy to accurately and repeatedly map foliar traits important for describing landscape patterns in nutrient cycling (e.g. Chapin 2003, Kazakou et al. 2006, Quested et al. 2007, Santiago 2007) and photosynthetic capacity (e.g. Kattge et al. 2009).The approach was robust across multiple traits, using data from numerous sites, vegetation types and years. Our method for estimating canopy chemistry integrated three scales of observation — leaf spectra, plot structure, image spectra —thus allowing the propagation of uncertainty from the leaf-level dependent variables to the plot/canopy level, and finally to maps created from image spectra. While imaging spectroscopy has been used in several

studies to map foliar traits (Wessman et al. 1989, Curran et al. 1997, Serrano et al. 2002, Townsend et al. 2003, Huber et al. 2008, Martin et al. 2008), ours demonstrates the capacity to map multiple functional traits across a diversity of sites, years, images, and geographic complexity, as well as explicitly accounting for the propagation of measurement, scaling, and modeling uncertainty through to the end product.

The per-trait waveband calibration coefficients provide a basis for physiological interpretation of the results as well as the assessment of the results' generality for mapping to other data sets. The important wavebands align with fresh-leaf results for M_{area} and dry sample results for chemical constituents reported by Serbin et al. (2012, 2014), as well as with wavebands indicated by Martin et al. (2008) as important for foliar nitrogen from AVIRIS (Fig. 5). In comparison with leaf-level results, standardized coefficients matched across most of the spectrum, but there was a reversal of sign in coefficients across the red-edge (500-700nm). Leaf-level NIR reflectance results from scattering at the interface between cell walls and intercellular air spaces, while canopy (i.e., image) reflectance is strongly dominated by canopy structural properties such as leaf clumping, angle, and density (Jacquemoud et al. 2009, Sullivan et al. 2013). For instance, leaf-level NIR reflectance generally increases with thickness of needle leaves (Ehleringer and Mooney 1978, Lin and Ehleringer 1983, DeLucia et al. 1996, Slaton et al. 2001), but canopy-level NIR reflectance decreases with greater abundance of needleleaf species because absorption-inducing canopy properties (e.g. greater needle clumping) overwhelm leaf traits in affecting NIR canopy reflectance (Ollinger 2011, Sullivan et al. 2013). Considering recent critiques of imaging spectroscopy-based trait mapping (Knyazikhin et al. 2013), this switch in the direction of NIR coefficients between leaf and canopy-level models of M_{area} provides added confidence that imaging spectroscopy captures sufficient information about the

canopy and constituent foliage for purposes of mapping (Ollinger et al. 2013, Townsend et al. 2013). Moreover, the striking similarity of results obtained from the four schemes to scale canopy height-related differences in measured leaf traits (Appendix A), further supports recent work emphasizing the mass-basis for measuring variability in the global leaf economics spectrum (Niinemets et al. 2014), and again underscores the robust ability of imaging spectroscopy to map spatial patterns from canopy-scale measurements.

We compared coefficients obtained from our analysis of %N with those published by Martin et al. (2008), the only other study using comparable multi-scene and multi-location data. Loadings of standardized coefficients for our models generally agreed with the Martin et al. models (2008) (Fig. 5). Discrepancies in locations of dips and spikes in coefficients result primarily from our use of a standardized dataset (i.e. centered and scaled) compared to raw coefficients from Martin et al. (2008). Martin et al. (2008) employed 11 images (5 AVIRIS, 6 Hyperion) covering a wide variety of temperate and tropical forest ecosystems in North America and Australia, and was the first to show the potential for building general models to map foliar traits across large regions.

While not as global in scope as Martin et al. (2008), our analysis incorporated multiple forest types dominated by a range of broadleaf and conifer species (Table A2, Appendix A, Supplement 1, Serbin et al. 2014), and covers the breadth of forest functional variability within North American eastern temperate forests. Any missing species and forest types are likely bracketed by the range of our data, and we expect that spatial patterns of uncertainties (e.g., Fig. 7) are indicative of gaps in our database for different forest optical types (sensu Ustin and Gamon 2010) rather than weaknesses in model performance. The largest uncertainties were observed in locations where 1) the vegetation was not represented in our database of foliar traits

422 due to our focus on forests (i.e. grasses, forbs, crops, wetlands); 2) there were strong terrain
423 effects in the imagery not fully accounted for in the topographic normalization; or 3) along forest
424 edges and disturbed areas. In particular, the uncertainty mapping helped identify areas that had
425 been recently disturbed (Appendix A, Fig A8). Logged areas showed a consistent pattern of
426 higher lignin and M_{area} and lower foliar nitrogen content (and also higher $\delta^{15}N$ indicating
427 increased N availability) compared to adjacent undisturbed areas. Although such patterns are not
428 unexpected, those areas also had consistently high uncertainties due to optical properties of
429 disturbances being on the edge ofthe range of variability of optical properties for the intact
430 forests we sampled. Future analysis of vegetation traits in disturbed areas using imaging
431 spectroscopy may provide the opportunity to better understand changes in ecosystem dynamics
432 brought about by human or natural perturbations.

433 Composite maps of functional traits (e.g., Appendix A, Fig A6) revealed a greater amount of
434 variability in forest canopies than apparent in individual maps, and in particular, landcover
435 classifications. For example, in the Central Appalachian sites, co-dominant conifers in ridges and
436 valleys were revealed by the higher lignin content and M_{area} of conifers (Fig.7). Comparisons
437 between maps of individual traits (Fig. 7) also revealed gradients in functional traits that follow
438 the inverse relationship between investments in leaf structural mass in contrast to leaf nutrients
439 (Wright and Westoby 2002, Reich et al. 2003, Wright et al. 2004). Regions showing higher foliar
440 nitrogen concentrations were associated with lower values of M_{area} and vice versa. While this is
441 widely known from multiple species inhabiting diverse ecosystems (Reich et al. 1998, Reich et al.
442 1999, Wright et al. 2001, Sanchez-Azofeifa et al. 2009, Asner et al. 2011b), imaging
443 spectroscopy allowed these associations to be mapped explicitly and across multiple ecoregions.

The geographic patterns in trait variability matched expectations associated with climate and other environmental drivers (Table 2). For example, the negative correlation between M_{area} and leaf nitrogen is in agreement with the broader concept of the leaf economic spectrum (Wright et al. 2004, Wright et al. 2005a, Wright et al. 2005b). The positive correlation of foliar N with regional scale N deposition corroborates evidence of foliar N enrichment reported in numerous studies in Northeastern forests (McNeil et al. 2007, Davis et al. 2009, Crowley et al. 2012, McNeil et al. 2012). Correlations of foliar $\delta^{15}N$ concentrations with mean annual temperature (positive) and precipitation (negative) agree with Amundson et al. (2003), Craine et al. (2009) and Serbin et al. (2014). Mapped evidence of increased isotopic N along the N deposition gradient corroborates Emmett et al. (1998) and McLauchlan et al. (2007), showing that greater N availability yields less preferential retention of lighter ^{14}N in the soil system.

It has been recently demonstrated that estimates of canopy structure and composition obtained from imaging spectroscopy are invaluable in constraining regional carbon flux models (Antonarakis et al. 2014). Maps of foliar traits obtained from this study can be leveraged to drive ecosystem process models requiring parameterization of foliar nitrogen content and leaf mass per area, which are coordinated in leaves to maximize carbon fixation (Shipley et al. 2005) in patterns independent of species-level physiognomy (Reich et al. 1991, Reich et al. 1992, Grime 2006).This offers the potential to develop datasets needed to drive spatially explicit ecosystem process models at large scales from proposed forthcoming satellites(e.g. HyspIRI, EnMAP: Stuffler et al. 2007, Middleton et al. 2013). While spatial patterns of canopy foliar N, lignin and M_{area} are largely interpretable in terms of species associations, patterns of $\delta^{15}N$ will require considerable follow-up field research. In locations where $\delta^{15}N$ concentrations appear elevated without associated increased uncertainties or changes in foliar N and or M_{area} (indicating an

obvious change in plant functional associations), localized patterns of $\delta^{15}N$ enrichment (for e.g. see SE corner in $\delta^{15}N$ map, Figure 7) could be an indicator of elevated N availability via ephemeral disturbances such as insect defoliation or logging. The availability of spatial predictions of foliar traits may therefore open up new investigations into biotic or abiotic nutrient cycling controls across both small regions and large landscapes.

Imaging spectroscopy offers the opportunity for applications ranging from assessment of biochemical effects of invasive species (Glenn et al. 2005, Asner et al. 2008, He et al. 2011), to characterizing photosynthetic down-regulation (Gamon et al. 1990, Gamon et al. 1992, Gamon et al. 1997) and measurement of the inductance of plant defense to perturbations (Couture et al. 2013). By directly measuring the chemical and physiological consequences of disturbances and other environmental drivers on vegetation, spaceborne imaging spectroscopy should provide the ability to directly quantify the consequences of environmental change rather than inferring it from landcover maps or vegetation indices. This will provide agencies the tools to measure impacts of invasions or help better guide management activities.

Conclusions

Using data from a wide range of forest ecosystems, we rigorously tested the capacity of imaging spectroscopy to map multiple forest functional traits. The resulting maps enable us to describe fundamental axes of variability in plant physiology along a spectrum ranging from "fast" (high nutrients and low lignin, thin, low M_{area} leaves) to "slow" patterns of forest nutrient cycling (Reich et al. 1991, Reich et al. 1992, Reich et al. 1999, Craine et al. 2002, Wright et al. 2005a, Wright et al. 2005b, Sanchez-Azofeifa et al. 2009). It is exciting to begin answering questions on the spatial patterns in these traits, but ultimately, trait mapping from imaging spectroscopy will

likely have its greatest impact by enabling researchers to pose more applied questions. For example: how does functional biogeography (Violle et al. 2014) mediate ecosystem response to environmental change? By helping answer such questions, multiple trait mapping, coupled with robust assessments of its uncertainty, opens up the potential for making defensible, tractable, and scalable predictions of the delivery of key ecosystem services from complex forest environments that are increasingly subjected to multiple agents of global environmental change.

Our work accomplishes two objectives: we provide a set of equations (supplements 2A-D) that can be used with imaging spectroscopy data to maps traits in similar environments (temperate forests). As well, we outline a workflow that could be implemented in other ecosystem types. An important next step for trait mapping is the integration of data collected from across the globe (Asner and Martin 2009, Asner et al. 2012). This integration will further determine the extent of the generality of these methods, with respect to sensor types, measurement or analytical strategies, and environmental variability. Coupled with other studies, this research represents a step toward the development of global approaches to mapping plant functional properties from imaging spectroscopy, and thus helps provide a more solid foundation for the development of "trait" products from the proposed HyspIRI mission and NEON's Aerial Observatory Platform (Kampe et al. 2010, Middleton et al. 2013, Sims et al. 2013).

Acknowledgements

AS and SPS were supported by graduate assistantships provided by NASA Terrestrial Ecology grant NNX08AN31G to PAT and BEM, and a NASA Earth and Space Science Fellowship grant NNX08AV07H to SPS. Thanks also to E. Kruger for helpful comments on earlier versions of this paper. The authors thank two anonymous reviewers for very constructive comments on the

manuscript.

References

Ainsworth, E. A., and A. Rogers. 2007. The response of photosynthesis and stomatal conductance to rising CO2 : mechanisms and environmental interactions. Plant Cell and Environment **30**:258-270.

Amundson, R., A. T. Austin, E. A. G. Schuur, K. Yoo, V. Matzek, C. Kendall, A. Uebersax, D. Brenner, and W. T. Baisden. 2003. Global patterns of the isotopic composition of soil and plant nitrogen. Global Biogeochemical Cycles **17**.

Antonarakis, A. S., J. W. Munger, and P. R. Moorcroft. 2014. Imaging spectroscopy- and lidar-derived estimates of canopy composition and structure to improve predictions of forest carbon fluxes and ecosystem dynamics. Geophysical Research Letters **41**:2535-2542.

Asner, G. P. 1998. Biophysical and biochemical sources of variability in canopy reflectance. Remote Sensing of Environment **64**:234-253.

Asner, G. P., M. O. Jones, R. E. Martin, D. E. Knapp, and R. F. Hughes. 2008. Remote sensing of native and invasive species in Hawaiian forests. Remote Sensing of Environment **112**:1912-1926.

Asner, G. P., D. E. Knapp, J. Boardman, R. O. Green, T. Kennedy-Bowdoin, M. Eastwood, R. E. Martin, C. Anderson, and C. B. Field. 2012. Carnegie Airborne Observatory-2: Increasing science data dimensionality via high-fidelity multi-sensor fusion. Remote Sensing of Environment **124**:454-465.

Asner, G. P., and R. E. Martin. 2008. Spectral and chemical analysis of tropical forests: Scaling from leaf to canopy levels. Remote Sensing of Environment **112**:3958-3970.

536 Asner, G. P., and R. E. Martin. 2009. Airborne spectranomics: mapping canopy chemical and
537 taxonomic diversity in tropical forests. Frontiers in Ecology and the Environment **7**:269-
538 276.
539 Asner, G. P., R. E. Martin, D. E. Knapp, R. Tupayachi, C. Anderson, L. Carranza, P. Martinez,
540 M. Houcheime, F. Sinca, and P. Weiss. 2011a. Spectroscopy of canopy chemicals in
541 humid tropical forests. Remote Sensing of Environment **115**:3587-3598.
542 Asner, G. P., R. E. Martin, R. Tupayachi, R. Emerson, P. Martinez, F. Sinca, G. V. N. Powell, S.
543 J. Wright, and A. E. Lugo. 2011b. Taxonomy and remote sensing of leaf mass per area
544 (LMA) in humid tropical forests. Ecological Applications **21**:85-98.
545 Asner, G. P., and P. M. Vitousek. 2005. Remote analysis of biological invasion and
546 biogeochemical change. Proceedings of the National Academy of Sciences of the United
547 States of America **102**:4383-4386.
548 Austin, A. T., and P. M. Vitousek. 1998. Nutrient dynamics on a precipitation gradient in
549 Hawai'i. Oecologia **113**:519-529.
550 Baret, F., V. C. Vanderbilt, M. D. Steven, and S. Jacquemoud. 1994. Use of spectral analogy to
551 evaluate canopy reflectance sensitivity to leaf optical-properties. Remote Sensing of
552 Environment **48**:253-260.
553 Berg, B. 2000. Litter decomposition and organic matter turnover in northern forest soils. Forest
554 Ecology and Management **133**:13-22.
555 Blackburn, G. A. 2007. Hyperspectral remote sensing of plant pigments. Journal of Experimental
556 Botany **58**:855-867.

557 Bonan, G. B. 1993. Physiological controls of the carbon balance of boreal forest ecosystems.
558 Canadian Journal of Forest Research-Revue Canadienne De Recherche Forestiere
559 **23**:1453-1471.
560 Canadell, J. G., C. Le Quere, M. R. Raupach, C. B. Field, E. T. Buitenhuis, P. Ciais, T. J.
561 Conway, N. P. Gillett, R. A. Houghton, and G. Marland. 2007. Contributions to
562 accelerating atmospheric CO(2) growth from economic activity, carbon intensity, and
563 efficiency of natural sinks. Proceedings of the National Academy of Sciences of the
564 United States of America **104**:18866-18870.
565 Carrera, A. L., and M. B. Bertiller. 2010. Relationships among plant litter, fine roots, and soil
566 organic C and N across an aridity gradient in northern Patagonia, Argentina. Ecoscience
567 **17**:276-286.
568 Chapin, F. S. 2003. Effects of plant traits on ecosystem and regional processes: a conceptual
569 framework for predicting the consequences of global change. Annals of Botany **91**:455-
570 463.
571 Chapin, F. S., M. S. BretHarte, S. E. Hobbie, and H. L. Zhong. 1996. Plant functional types as
572 predictors of transient responses of arctic vegetation to global change. Journal of
573 Vegetation Science **7**:347-358.
574 Chen, S., X. Hong, C. J. Harris, and P. M. Sharkey. 2004. Sparse modeling using orthogonal
575 forward regression with PRESS statistic and regularization. Ieee Transactions on Systems
576 Man and Cybernetics Part B-Cybernetics **34**:898-911.
577 Collatz, G. J., M. Ribas-Carbo, and J. A. Berry. 1992. Coupled photosynthesis-stomatal
578 conductance model for leaves of C4 plants. Australian Journal of Plant Physiology
579 **19**:519-538.

Coops, N. C., M. L. Smith, M. E. Martin, and S. V. Ollinger. 2003. Prediction of eucalypt foliage nitrogen content from satellite-derived hyperspectral data. Ieee Transactions on Geoscience and Remote Sensing **41**:1338-1346.

Couture, J. J., S. P. Serbin, and P. A. Townsend. 2013. Spectroscopic sensitivity of real-time, rapidly induced phytochemical change in response to damage. New Phytologist **198**:311-319.

Craine, J. M., A. J. Elmore, M. P. M. Aidar, M. Bustamante, T. E. Dawson, E. A. Hobbie, A. Kahmen, M. C. Mack, K. K. McLauchlan, A. Michelsen, G. B. Nardoto, L. H. Pardo, J. Penuelas, P. B. Reich, E. A. G. Schuur, W. D. Stock, P. H. Templer, R. A. Virginia, J. M. Welker, and I. J. Wright. 2009. Global patterns of foliar nitrogen isotopes and their relationships with climate, mycorrhizal fungi, foliar nutrient concentrations, and nitrogen availability. New Phytologist **183**:980-992.

Craine, J. M., D. Tilman, D. Wedin, P. Reich, M. Tjoelker, and J. Knops. 2002. Functional traits, productivity and effects on nitrogen cycling of 33 grassland species. Functional Ecology **16**:563-574.

Cramer, W., A. Bondeau, F. I. Woodward, I. C. Prentice, R. A. Betts, V. Brovkin, P. M. Cox, V. Fisher, J. A. Foley, A. D. Friend, C. Kucharik, M. R. Lomas, N. Ramankutty, S. Sitch, B. Smith, A. White, and C. Young-Molling. 2001. Global response of terrestrial ecosystem structure and function to CO2 and climate change: results from six dynamic global vegetation models. Global Change Biology **7**:357-373.

Crowley, K. F., B. E. McNeil, G. M. Lovett, C. D. Canham, C. T. Driscoll, L. E. Rustad, E. Denny, R. A. Hallett, M. A. Arthur, J. L. Boggs, C. L. Goodale, J. S. Kahl, S. G. McNulty, S. V. Ollinger, L. H. Pardo, P. G. Schaberg, J. L. Stoddard, M. P. Weand, and

K. C. Weathers. 2012. Do nutrient limitation patterns shift from nitrogen toward phosphorus with increasing nitrogen deposition across the northeastern United States? Ecosystems **15**:940-957.

Curran, P. J. 1989. Remote-sensing of foliar chemistry. Remote Sensing of Environment **30**:271-278.

Curran, P. J., J. L. Dungan, B. A. Macler, S. E. Plummer, and D. L. Peterson. 1992. Reflectance spectroscopy of fresh whole leaves for the estimation of chemical concentration. Remote Sensing of Environment **39**:153-166.

Curran, P. J., J. L. Dungan, and D. L. Peterson. 2001. Estimating the foliar biochemical concentration of leaves with reflectance spectrometry testing the Kokaly and Clark methodologies. Remote Sensing of Environment **76**:349-359.

Curran, P. J., J. A. Kupiec, and G. M. Smith. 1997. Remote sensing the biochemical composition of a slash pine canopy. Ieee Transactions on Geoscience and Remote Sensing **35**:415-420.

Davis, S. C., K. E. Dragan, C. R. Buyarski, and R. B. Thomas. 2009. High foliar and soil nitrogen concentrations in central Appalachian forests. Ecosystems **12**:46-56.

Deel, L. N., B. E. McNeil, P. G. Curtis, S. P. Serbin, A. Singh, K. N. Eshleman, and P. A. Townsend. 2012. Relationship of a Landsat cumulative disturbance index to canopy nitrogen and forest structure. Remote Sensing of Environment **118**:40-49.

DeLucia, E. H., K. Nelson, T. C. Vogelmann, and W. K. Smith. 1996. Contribution of intercellular reflectance to photosynthesis in shade leaves. Plant Cell and Environment **19**:159-170.

Diaz, S., J. G. Hodgson, K. Thompson, M. Cabido, J. H. C. Cornelissen, A. Jalili, G. Montserrat-Marti, J. P. Grime, F. Zarrinkamar, Y. Asri, S. R. Band, S. Basconcelo, P. Castro-Diez, G.

626 Funes, B. Hamzehee, M. Khoshnevi, N. Perez-Harguindeguy, M. C. Perez-Rontome, F.
627 A. Shirvany, F. Vendramini, S. Yazdani, R. Abbas-Azimi, A. Bogaard, S. Boustani, M.
628 Charles, M. Dehghan, L. de Torres-Espuny, V. Falczuk, J. Guerrero-Campo, A. Hynd, G.
629 Jones, E. Kowsary, F. Kazemi-Saeed, M. Maestro-Martinez, A. Romo-Diez, S. Shaw, B.
630 Siavash, P. Villar-Salvador, and M. R. Zak. 2004. The plant traits that drive ecosystems:
631 Evidence from three continents. Journal of Vegetation Science **15**:295-304.
632 Ehleringer, J. R., and H. A. Mooney. 1978. Leaf hairs - effects on physiological-activity and
633 adaptive value to a desert shrub. Oecologia **37**:183-200.
634 Emmett, B. A., O. J. Kjonaas, P. Gundersen, C. Koopmans, A. Tietema, and D. Sleep. 1998.
635 Natural abundance of N-15 in forests across a nitrogen deposition gradient. Forest
636 Ecology and Management **101**:9-18.
637 Enquist, B. J., A. J. Kerkhoff, T. E. Huxman, and E. P. Economo. 2007. Adaptive differences in
638 plant physiology and ecosystem paradoxes: insights from metabolic scaling theory.
639 Global Change Biology **13**:591-609.
640 Fortunel, C., E. Garnier, R. Joffre, E. Kazakou, H. Quested, K. Grigulis, S. Lavorel, P. Ansquer,
641 H. Castro, P. Cruz, J. Dolezal, O. Eriksson, H. Freitas, C. Golodets, C. Jouany, J. Kigel,
642 M. Kleyer, V. Lehsten, J. Leps, T. Meier, R. Pakeman, M. Papadimitriou, V. P.
643 Papanastasis, F. Quetier, M. Robson, M. Sternberg, J. P. Theau, A. Thebault, and M.
644 Zarovali. 2009. Leaf traits capture the effects of land use changes and climate on litter
645 decomposability of grasslands across Europe. Ecology **90**:598-611.
646 Fourty, T., F. Baret, S. Jacquemoud, G. Schmuck, and J. Verdebout. 1996. Leaf optical
647 properties with explicit description of its biochemical composition: Direct and inverse
648 problems. Remote Sensing of Environment **56**:104-117.

649 Frank, I. E., and J. H. Friedman. 1993. A statistical view of some chemometrics regression tools.
650 Technometrics **35**:109-135.
651 Friedlingstein, P., R. M. Andrew, J. Rogelj, G. P. Peters, J. G. Canadell, R. Knutti, G. Luderer,
652 M. R. Raupach, M. Schaeffer, D. P. van Vuuren, and C. Le Quéré. 2014. Persistent
653 growth of CO_2 emissions and implications for reaching climate targets. Nature
654 Geoscience **7**:709-715.
655 Gamon, J. A., C. B. Field, W. Bilger, O. Bjorkman, A. L. Fredeen, and J. Penuelas. 1990.
656 Remote-sensing of the xanthophyll cycle and chlorophyll fluorescence in sunflower
657 leaves and canopies. Oecologia **85**:1-7.
658 Gamon, J. A., J. Penuelas, and C. B. Field. 1992. A narrow-waveband spectral index that tracks
659 diurnal changes in photosynthetic efficiency. Remote Sensing of Environment **41**:35-44.
660 Gamon, J. A., L. Serrano, and J. S. Surfus. 1997. The photochemical reflectance index: an
661 optical indicator of photosynthetic radiation use efficiency across species, functional
662 types, and nutrient levels. Oecologia **112**:492-501.
663 Gao, B. C., M. J. Montes, Z. Ahmad, and C. O. Davis. 2000. Atmospheric correction algorithm
664 for hyperspectral remote sensing of ocean color from space. Applied Optics **39**:887-896.
665 Gates, D. M., H. J. Keegan, J. C. Schleter, and V. R. Weidner. 1965. Spectral properties of plants.
666 Applied Optics **4**:11-&.
667 Geladi, P., and B. R. Kowalski. 1986. Partial least-squares regression - a tutorial. Analytica
668 Chimica Acta **185**:1-17.
669 Glenn, N. F., J. T. Mundt, K. T. Weber, T. S. Prather, L. W. Lass, and J. Pettingill. 2005.
670 Hyperspectral data processing for repeat detection of small infestations of leafy spurge.
671 Remote Sensing of Environment **95**:399-412.

672 Green, D. S., J. E. Erickson, and E. L. Kruger. 2003. Foliar morphology and canopy nitrogen as
673 predictors of light-use efficiency in terrestrial vegetation. Agricultural and Forest
674 Meteorology **115**:163-171.
675 Green, R. O., M. L. Eastwood, C. M. Sarture, T. G. Chrien, M. Aronsson, B. J. Chippendale, J. A.
676 Faust, B. E. Pavri, C. J. Chovit, M. S. Solis, M. R. Olah, and O. Williams. 1998. Imaging
677 spectroscopy and the Airborne Visible Infrared Imaging Spectrometer (AVIRIS). Remote
678 Sensing of Environment **65**:227-248.
679 Grime, J. P. 2006. Trait convergence and trait divergence in herbaceous plant communities:
680 Mechanisms and consequences. Journal of Vegetation Science **17**:255-260.
681 Grossman, Y. L., S. L. Ustin, S. Jacquemoud, E. W. Sanderson, G. Schmuck, and J. Verdebout.
682 1996. Critique of stepwise multiple linear regression for the extraction of leaf
683 biochemistry information from leaf reflectance data. Remote Sensing of Environment
684 **56**:182-193.
685 Hattenschwiler, S., A. V. Tiunov, and S. Scheu. 2005. Biodiversity and litter decomposition
686 interrestrial ecosystems. Pages 191-218 Annual Review of Ecology Evolution and
687 Systematics.
688 He, K. S., D. Rocchini, M. Neteler, and H. Nagendra. 2011. Benefits of hyperspectral remote
689 sensing for tracking plant invasions. Diversity and Distributions **17**:381-392.
690 Hobbie, E. A., S. A. Macko, and M. Williams. 2000. Correlations between foliar delta N-15 and
691 nitrogen concentrations may indicate plant-mycorrhizal interactions. Oecologia **122**:273-
692 283.

693 Hobbie, S. E., M. Ogdahl, J. Chorover, O. A. Chadwick, J. Oleksyn, R. Zytkowiak, and P. B.
694 Reich. 2007. Tree species effects on soil organic matter dynamics: The role of soil cation
695 composition. Ecosystems **10**:999-1018.
696 Hogberg, P. 1997. Tansley review No 95 - N-15 natural abundance in soil-plant systems. New
697 Phytologist **137**:179-203.
698 Huber, S., M. Kneubuhler, A. Psomas, K. Itten, and N. E. Zimmermann. 2008. Estimating foliar
699 biochemistry from hyperspectral data in mixed forest canopy. Forest Ecology and
700 Management **256**:491-501.
701 Jenkins, J. C., D. C. Chojnacky, L. S. Heath, and R. A. Birdsey. 2003. National-scale biomass
702 estimators for United States tree species. Forest Science **49**:12-35.
703 Johnson, J. M. F., N. W. Barbour, and S. L. Weyers. 2007. Chemical composition of crop
704 biomass impacts its decomposition. Soil Science Society of America Journal **71**:155-162.
705 Kampe, T. U., B. R. Johnson, M. Kuester, and M. Keller. 2010. NEON: the first continental-
706 scale ecological observatory with airborne remote sensing of vegetation canopy
707 biochemistry and structure. Journal of Applied Remote Sensing **4**.
708 Kattge, J., W. Knorr, T. Raddatz, and C. Wirth. 2009. Quantifying photosynthetic capacity and
709 its relationship to leaf nitrogen content for global-scale terrestrial biosphere models.
710 Global Change Biology **15**:976-991.
711 Kazakou, E., D. Vile, B. Shipley, C. Gallet, and E. Garnier. 2006. Co-variations in litter
712 decomposition, leaf traits and plant growth in species from a Mediterranean old-field
713 succession. Functional Ecology **20**:21-30.

714 Kazakou, E., C. Violle, C. Roumet, C. Pintor, O. Gimenez, and E. Garnier. 2009. Litter quality
715 and decomposability of species from a Mediterranean succession depend on leaf traits but
716 not on nitrogen supply. Annals of Botany **104**:1151-1161.
717 Kergoat, L., S. Lafont, A. Arneth, V. Le Dantec, and B. Saugier. 2008. Nitrogen controls plant
718 canopy light-use efficiency in temperate and boreal ecosystems. Journal of Geophysical
719 Research-Biogeosciences **113**.
720 Knorr, M., S. D. Frey, and P. S. Curtis. 2005. Nitrogen additions and litter decomposition: A
721 meta-analysis. Ecology **86**:3252-3257.
722 Knyazikhin, Y., M. A. Schull, P. Stenberg, M. Mottus, M. Rautiainen, Y. Yang, A. Marshak, P.
723 L. Carmona, R. K. Kaufmann, P. Lewis, M. I. Disney, V. Vanderbilt, A. B. Davis, F.
724 Baret, S. Jacquemoud, A. Lyapustin, and R. B. Myneni. 2013. Hyperspectral remote
725 sensing of foliar nitrogen content. Proceedings of the National Academy of Sciences of
726 the United States of America **110**:E185-E192.
727 Kokaly, R. F. 2001. Investigating a physical basis for spectroscopic estimates of leaf nitrogen
728 concentration. Remote Sensing of Environment **75**:153-161.
729 Kokaly, R. F., G. P. Asner, S. V. Ollinger, M. E. Martin, and C. A. Wessman. 2009.
730 Characterizing canopy biochemistry from imaging spectroscopy and its application to
731 ecosystem studies. Remote Sensing of Environment **113**:S78-S91.
732 Le Quere, C., M. R. Raupach, J. G. Canadell, G. Marland, L. Bopp, P. Ciais, T. J. Conway, S. C.
733 Doney, R. A. Feely, P. Foster, P. Friedlingstein, K. Gurney, R. A. Houghton, J. I. House,
734 C. Huntingford, P. E. Levy, M. R. Lomas, J. Majkut, N. Metzl, J. P. Ometto, G. P. Peters,
735 I. C. Prentice, J. T. Randerson, S. W. Running, J. L. Sarmiento, U. Schuster, S. Sitch, T.

736 Takahashi, N. Viovy, G. R. van der Werf, and F. I. Woodward. 2009. Trends in the
737 sources and sinks of carbon dioxide. Nature Geoscience **2**:831-836.
738 Lilleskov, E. A., E. A. Hobbie, and T. J. Fahey. 2002. Ectomycorrhizal fungal taxa differing in
739 response to nitrogen deposition also differ in pure culture organic nitrogen use and
740 natural abundance of nitrogen isotopes. New Phytologist **154**:219-231.
741 Lin, Z. F., and J. Ehleringer. 1983. Epidermis effects on spectral properties of leaves of 4
742 herbaceous species. Physiologia Plantarum **59**:91-94.
743 Long, S. P. 1991. Modification of the response of photosynthetic productivity to rising
744 temperature by atmospheric CO_2 concentrations - has its importance been underestimated.
745 Plant Cell and Environment **14**:729-739.
746 Lucht, W., C. B. Schaaf, and A. H. Strahler. 2000. An algorithm for the retrieval of albedo from
747 space using semiempirical BRDF models. Ieee Transactions on Geoscience and Remote
748 Sensing **38**:977-998.
749 Martin, M. E., and J. D. Aber. 1997. High spectral resolution remote sensing of forest canopy
750 lignin, nitrogen, and ecosystem processes. Ecological Applications **7**:431-443.
751 Martin, M. E., L. C. Plourde, S. V. Ollinger, M. L. Smith, and B. E. McNeil. 2008. A
752 generalizable method for remote sensing of canopy nitrogen across a wide range of forest
753 ecosystems. Remote Sensing of Environment **112**:3511-3519.
754 Martinelli, L. A., M. C. Piccolo, A. R. Townsend, P. M. Vitousek, E. Cuevas, W. McDowell, G.
755 P. Robertson, O. C. Santos, and K. Treseder. 1999. Nitrogen stable isotopic composition
756 of leaves and soil: Tropical versus temperate forests. Biogeochemistry **46**:45-65.

757 Matson, P., L. Johnson, C. Billow, J. Miller, and R. L. Pu. 1994. Seasonal patterns and remote
758 spectral estimation of canopy chemistry across the Oregon transect. Ecological
759 Applications **4**:280-298.
760 McClaugherty, C., and B. Berg. 1987. Cellulose, lignin and nitrogen concentrations as rate
761 regulating factors in late stages of forest litter decomposition. Pedobiologia **30**:101-112.
762 McLauchlan, K. K., J. M. Craine, W. W. Oswald, P. R. Leavitt, and G. E. Likens. 2007. Changes
763 in nitrogen cycling during the past century in a northern hardwood forest. Proceedings of
764 the National Academy of Sciences of the United States of America **104**:7466-7470.
765 McNeil, B. E., K. M. de Beurs, K. N. Eshleman, J. R. Foster, and P. A. Townsend. 2007.
766 Maintenance of ecosystem nitrogen limitation by ephemeral forest disturbance: An
767 assessment using MODIS, Hyperion, and Landsat ETM. Geophysical Research Letters
768 **34**:-.
769 McNeil, B. E., J. M. Read, and C. T. Driscoll. 2012. Foliar Nitrogen Responses to the
770 Environmental Gradient Matrix of the Adirondack Park, New York. Annals of the
771 Association of American Geographers **102**:1-16.
772 McNeil, B. E., J. M. Read, T. J. Sullivan, T. C. McDonnell, I. J. Fernandez, and C. T. Driscoll.
773 2008. The spatial pattern of nitrogen cycling in the Adirondack Park, New York.
774 Ecological Applications **18**:438-452.
775 Meier, C. L., and W. D. Bowman. 2008. Links between plant litter chemistry, species diversity,
776 and below-ground ecosystem function. Proceedings of the National Academy of Sciences
777 of the United States of America **105**:19780-19785.
778 Melillo, J. M., J. D. Aber, and J. F. Muratore. 1982. Nitrogen and lignin control of hardwood leaf
779 litter decomposition dynamics. Ecology **63**:621-626.

780 Menesatti, P., F. Antonucci, F. Pallottino, G. Roccuzzo, M. Allegra, F. Stagno, and F. Intrigliolo.
781 2010. Estimation of plant nutritional status by Vis-NIR spectrophotometric analysis on
782 orange leaves Citrus sinensis (L) Osbeck cv Tarocco. Biosystems Engineering **105**:448-
783 454.
784 Middleton, E. M., S. G. Ungar, D. J. Mandl, L. Ong, S. W. Frye, P. E. Campbell, D. R. Landis, J.
785 P. Young, and N. H. Pollack. 2013. The Earth Observing One (EO-1) Satellite Mission:
786 Over a Decade in Space. Ieee Journal of Selected Topics in Applied Earth Observations
787 and Remote Sensing **6**:243-256.
788 Montes, M. J., and B.-C. Gao. 2004. NRL Atmospheric Correction Algorithms for Oceans:
789 TAFKAA Users' Guide.
790 NADP. 2014. National Atmospheric Deposition Program NADP Program Office, Illinois State
791 Water Survey, 2204 Griffith Dr., Champaign, IL 61820.
792 Niinemets, U. 2001. Global-scale climatic controls of leaf dry mass per area, density, and
793 thickness in trees and shrubs. Ecology **82**:453-469.
794 Niinemets, Ü., T. F. Keenan, and L. Hallik. 2014. A worldwide analysis of within-canopy
795 variations in leaf structural, chemical and physiological traits across plant functional
796 types. New Phytologist.
797 Ollinger, S. V. 2011. Sources of variability in canopy reflectance and the convergent properties
798 of plants. New Phytologist **189**:375-394.
799 Ollinger, S. V., P. B. Reich, S. Frolking, L. C. Lepine, D. Y. Hollinger, and A. D. Richardson.
800 2013. Nitrogen cycling, forest canopy reflectance, and emergent properties of ecosystems.
801 Proceedings of the National Academy of Sciences of the United States of America
802 **110**:E2437-E2437.

Ollinger, S. V., M. L. Smith, M. E. Martin, R. A. Hallett, C. L. Goodale, and J. D. Aber. 2002. Regional variation in foliar chemistry and N cycling among forests of diverse history and composition. Ecology **83**:339-355.

Petisco, C., B. Garcia-Criado, S. Mediavilla, B. R. V. de Aldana, I. Zabalgogeazcoa, and A. Garcia-Ciudad. 2006. Near-infrared reflectance spectroscopy as a fast and non-destructive tool to predict foliar organic constituents of several woody species. Analytical and Bioanalytical Chemistry **386**:1823-1833.

PRISM. 2004. PRISM Climate Group. Oregon State University.

Quested, H., O. Eriksson, C. Fortunel, and E. Garnier. 2007. Plant traits relate to whole-community litter quality and decomposition following land use change. Functional Ecology **21**:1016-1026.

Reich, P. B., D. S. Ellsworth, and M. B. Walters. 1998. Leaf structure (specific leaf area) modulates photosynthesis-nitrogen relations: evidence from within and across species and functional groups. Functional Ecology **12**:948-958.

Reich, P. B., D. S. Ellsworth, M. B. Walters, J. M. Vose, C. Gresham, J. C. Volin, and W. D. Bowman. 1999. Generality of leaf trait relationships: A test across six biomes. Ecology **80**:1955-1969.

Reich, P. B., C. Uhl, M. B. Walters, and D. S. Ellsworth. 1991. Leaf life-span as a determinant of leaf structure and function among 23 Amazonian tree species. Oecologia **86**:16-24.

Reich, P. B., M. B. Walters, and D. S. Ellsworth. 1992. Leaf life-span in relation to leaf, plant, and stand characteristics among diverse ecosystems Ecological Monographs **62**:365-392.

824 Reich, P. B., M. B. Walters, and D. S. Ellsworth. 1997. From tropics to tundra: Global
825 convergence in plant functioning. Proceedings of the National Academy of Sciences of
826 the United States of America **94**:13730-13734.
827 Reich, P. B., I. J. Wright, J. Cavender-Bares, J. M. Craine, J. Oleksyn, M. Westoby, and M. B.
828 Walters. 2003. The evolution of plant functional variation: Traits, spectra, and strategies.
829 International Journal of Plant Sciences **164**:S143-S164.
830 Richardson, A. D., and J. B. Reeves. 2005. Quantitative reflectance spectroscopy as an
831 alternative to traditional wet lab analysis of foliar chemistry: near-infrared and mid-
832 infrared calibrations compared. Canadian Journal of Forest Research-Revue Canadienne
833 De Recherche Forestiere **35**:1122-1130.
834 Ripullone, F., G. Grassi, M. Lauteri, and M. Borghetti. 2003. Photosynthesis-nitrogen
835 relationships: interpretation of different patterns between Pseudotsuga menziesii and
836 Populus x euroamericana in a mini-stand experiment. Tree Physiology **23**:137-144.
837 Robinson, D. 2001. delta N-15 as an integrator of the nitrogen cycle. Trends in Ecology &
838 Evolution **16**:153-162.
839 Roujean, J. L., M. Leroy, and P. Y. Deschamps. 1992. A bidirectional reflectance model of the
840 earth's surface for the correction of remote sensing data Journal of Geophysical Research
841 **97**:20455-20468.
842 Sanchez-Azofeifa, G. A., K. Castro, S. J. Wright, J. Gamon, M. Kalacska, B. Rivard, S. A.
843 Schnitzer, and J. L. Feng. 2009. Differences in leaf traits, leaf internal structure, and
844 spectral reflectance between two communities of lianas and trees: Implications for remote
845 sensing in tropical environments. Remote Sensing of Environment **113**:2076-2088.

Santiago, L. S. 2007. Extending the leaf economics spectrum to decomposition: Evidence from a tropical forest. Ecology **88**:1126-1131.

Santiago, L. S., K. Kitajima, S. J. Wright, and S. S. Mulkey. 2004. Coordinated changes in photosynthesis, water relations and leaf nutritional traits of canopy trees along a precipitation gradient in lowland tropical forest. Oecologia **139**:495-502.

Schimel, D. S. 1995. Terrestrial ecosystems and the carbon-cycle. Global Change Biology **1**:77-91.

Scott, N. A., and D. Binkley. 1997. Foliage litter quality and annual net N mineralization: Comparison across North American forest sites. Oecologia **111**:151-159.

Serbin, S. P., D. N. Dillaway, E. L. Kruger, and P. A. Townsend. 2012. Leaf optical properties reflect variation in photosynthetic metabolism and its sensitivity to temperature. Journal of Experimental Botany **63**:489-502.

Serbin, S. P., A. Singh, B. E. McNeil, C. C. Kingdon, and P. A. Townsend. 2014. Spectroscopic determination of leaf morphological and biochemical traits for northern temperate and boreal tree species. Ecological Applications.

Serrano, L., J. Penuelas, and S. L. Ustin. 2002. Remote sensing of nitrogen and lignin in Mediterranean vegetation from AVIRIS data: Decomposing biochemical from structural signals. Remote Sensing of Environment **81**:355-364.

Shipley, B., and M. J. Lechowicz. 2000. The functional co-ordination of leaf morphology, nitrogen concentration, and gas exchange in 40 wetland species. Ecoscience **7**:183-194.

Shipley, B., M. J. Lechowicz, I. Wright, and P. B. Reich. 2006. Fundamental trade-offs generating the worldwide leaf economics spectrum. Ecology **87**:535-541.

868 Shipley, B., D. Vile, E. Garnier, I. J. Wright, and H. Poorter. 2005. Functional linkages between
869 leaf traits and net photosynthetic rate: reconciling empirical and mechanistic models.
870 Functional Ecology **19**:602-615.
871 Sims, D. A., and J. A. Gamon. 2002. Relationships between leaf pigment content and spectral
872 reflectance across a wide range of species, leaf structures and developmental stages.
873 Remote Sensing of Environment **81**:337-354.
874 Sims, N. C., D. Culvenor, G. Newnham, N. C. Coops, and P. Hopmans. 2013. Towards the
875 Operational Use of Satellite Hyperspectral Image Data for Mapping Nutrient Status and
876 Fertilizer Requirements in Australian Plantation Forests. Ieee Journal of Selected Topics
877 in Applied Earth Observations and Remote Sensing **6**:320-328.
878 Slaton, M. R., E. R. Hunt, and W. K. Smith. 2001. Estimating near-infrared leaf reflectance from
879 leaf structural characteristics. American Journal of Botany **88**:278-284.
880 Smith, M. L., M. E. Martin, L. Plourde, and S. V. Ollinger. 2003. Analysis of hyperspectral data
881 for estimation of temperate forest canopy nitrogen concentration: Comparison between an
882 airborne (AVIRIS) and a spaceborne (Hyperion) sensor. Ieee Transactions on Geoscience
883 and Remote Sensing **41**:1332-1337.
884 Soenen, S. A., D. R. Peddle, and C. A. Coburn. 2005. SCS+C: A modified sun-canopy-sensor
885 topographic correction in forested terrain. Ieee Transactions on Geoscience and Remote
886 Sensing **43**:2148-2159.
887 Stuffler, T., C. Kaufmann, S. Hofer, K. P. Forster, G. Schreier, A. Mueller, A. Eckardt, H. Bach,
888 B. Penne, U. Benz, and R. Haydn. 2007. The EnMAP hyperspectral imager- An advanced
889 optical payload for future applications in Earth observation programmes. Acta
890 Astronautica **61**:115-120.

Sullivan, F. B., S. V. Ollinger, M. E. Martin, M. J. Ducey, L. C. Lepine, and H. F. Wicklein. 2013. Foliar nitrogen in relation to plant traits and reflectance properties of New Hampshire forests. Canadian Journal of Forest Research-Revue Canadienne De Recherche Forestiere **43**:18-27.

Townsend, A. R., G. P. Asner, and C. C. Cleveland. 2008. The biogeochemical heterogeneity of tropical forests. Trends in Ecology & Evolution **23**:424-431.

Townsend, P. A., J. R. Foster, R. A. Chastain, and W. S. Currie. 2003. Application of imaging spectroscopy to mapping canopy nitrogen in the forests of the central Appalachian Mountains using Hyperion and AVIRIS. Ieee Transactions on Geoscience and Remote Sensing **41**:1347-1354.

Townsend, P. A., S. P. Serbin, E. L. Kruger, and J. A. Gamon. 2013. Disentangling the contribution of biological and physical properties of leaves and canopies in imaging spectroscopy data. Proceedings of the National Academy of Sciences of the United States of America **110**:E1074-E1074.

Tucker, C. J. 1980. Remote-sensing of leaf water-content in the near-infrared. Remote Sensing of Environment **10**:23-32.

Ustin, S. L., and J. A. Gamon. 2010. Remote sensing of plant functional types. New Phytologist **186**:795-816.

Ustin, S. L., D. Riano, and E. R. Hunt. 2012. Estimating canopy water content from spectroscopy. Israel Journal of Plant Sciences **60**:9-23.

Vane, G., R. O. Green, T. G. Chrien, H. T. Enmark, E. G. Hansen, and W. M. Porter. 1993. The Airborne Visible Infrared Imaging Spectrometer (AVIRIS). Remote Sensing of Environment **44**:127-143.

914 Violle, C., E. Garnier, J. Lecoeur, C. Roumet, C. Podeur, A. Blanchard, and M. L. Navas. 2009.
915 Competition, traits and resource depletion in plant communities. Oecologia **160**:747-755.
916 Violle, C., P. B. Reich, S. W. Pacala, B. J. Enquist, and J. Kattge. 2014. The emergence and
917 promise of functional biogeography. Proceedings of the National Academy of Sciences of
918 the United States of America **111**:13690-13696.
919 Wessman, C. A., J. D. Aber, and D. L. Peterson. 1989. An evaluation of imaging spectrometry
920 for estimating forest canopy chemistry. International Journal of Remote Sensing **10**:1293-
921 1316.
922 Wold, S. 1994. PLS for Multivariate Linear Modeling. Page 359 *in* H. Waterbeemd, H.
923 Timmerman, R. Mannhold, and P. Kroqsgaard-Larsen, editors. QSAR: Chemometric
924 Methods in Molecular Design. Methods and Principles in Medicinal Chemistry. Wiley.
925 Wold, S., A. Ruhe, H. Wold, and W. J. Dunn. 1984. The Collinearity Problem in Linear-
926 Regression - the Partial Least-Squares (Pls) Approach to Generalized Inverses. Siam
927 Journal on Scientific and Statistical Computing **5**:735-743.
928 Wold, S., M. Sjostrom, and L. Eriksson. 2001. PLS-regression: a basic tool of chemometrics.
929 Chemometrics and Intelligent Laboratory Systems **58**:109-130.
930 Wolter, P. T., P. A. Townsend, B. R. Sturtevant, and C. C. Kingdon. 2008. Remote sensing of
931 the distribution and abundance of host species for spruce budworm in Northern
932 Minnesota and Ontario. Remote Sensing of Environment **112**:3971-3982.
933 Wright, I. J., P. B. Reich, J. H. C. Cornelissen, D. S. Falster, E. Garnier, K. Hikosaka, B. B.
934 Lamont, W. Lee, J. Oleksyn, N. Osada, H. Poorter, R. Villar, D. I. Warton, and M.
935 Westoby. 2005a. Assessing the generality of global leaf trait relationships. New
936 Phytologist **166**:485-496.

Wright, I. J., P. B. Reich, J. H. C. Cornelissen, D. S. Falster, P. K. Groom, K. Hikosaka, W. Lee, C. H. Lusk, U. Niinemets, J. Oleksyn, N. Osada, H. Poorter, D. I. Warton, and M. Westoby. 2005b. Modulation of leaf economic traits and trait relationships by climate. Global Ecology and Biogeography **14**:411-421.

Wright, I. J., P. B. Reich, and M. Westoby. 2001. Strategy shifts in leaf physiology, structure and nutrient content between species of high- and low-rainfall and high- and low-nutrient habitats. Functional Ecology **15**:423-434.

Wright, I. J., P. B. Reich, M. Westoby, D. D. Ackerly, Z. Baruch, F. Bongers, J. Cavender-Bares, T. Chapin, J. H. C. Cornelissen, M. Diemer, J. Flexas, E. Garnier, P. K. Groom, J. Gulias, K. Hikosaka, B. B. Lamont, T. Lee, W. Lee, C. Lusk, J. J. Midgley, M. L. Navas, U. Niinemets, J. Oleksyn, N. Osada, H. Poorter, P. Poot, L. Prior, V. I. Pyankov, C. Roumet, S. C. Thomas, M. G. Tjoelker, E. J. Veneklaas, and R. Villar. 2004. The worldwide leaf economics spectrum. Nature **428**:821-827.

Wright, I. J., and M. Westoby. 2002. Leaves at low versus high rainfall: coordination of structure, lifespan and physiology. New Phytologist **155**:403-416.

Yoder, B. J., and R. E. Pettigrewcrosby. 1995. Predicting nitrogen and chlorophyll content and concentrations from reflectance spectra (400-2500 nm) at leaf and canopy scales. Remote Sensing of Environment **53**:199-211.

Ecological Archives

Appendix A: Comparisons of model accuracies with literature, species-wise estimates of canopy foliar traits,comparisons of models built with different canopy weighing schemes, comparisons of spatial predictions of foliar traits.

Supplement 1: Plot locations, dominant and subdominant species and their relative basal areas, foliar traits measured in this study.

Supplement 2A: PLSR coefficients (500 each) for foliar traits described in this paper using canopy estimates aggregated with 90%, 9% and 1% weightage for top, middle and bottom canopy positions respectively.

Supplement 2B: PLSR coefficients (500 each) for foliar traits described in this paper using canopy estimates aggregated with 64.5%, 32.3% and 3.2% weightage for top, middle and bottom canopy positions respectively.

Supplement 2C: PLSR coefficients (500 each) for foliar traits described in this paper using canopy estimates aggregated with 40%, 40% and 20% weightage for top, middle and bottom canopy positions respectively.

Supplement 2D: PLSR coefficients (500 each) for foliar traits described in this paper using canopy estimates aggregated with 100% weightage for the top canopy.

974

975 ## Tables

976 **Table1** Summary statistics for canopy-level nutritional and morphological traits examined in this study. Means, standard deviations

977 and ranges of canopy foliar traits are presented aggregated across 237 plots sampled from 2008-2011.

978

	Overall		Needleleaf		Broadleaf	
Trait	Mean (SD)	Range	Mean (SD)	Range	Mean (SD)	Range
$M_{area}(g/m_2)$	116.23 (44.81)	51.88 – 313.44	168.33 (29.00)	101.24 – 313.44	86.90 (16.47)	51.88 – 151.55
N%	2.20 (0.58)	0.96 – 3.31	1.60 (0.30)	0.96 – 2.48	2.54 (0.39)	1.20 – 3.31
C%	49.83 (1.14)	46.39 – 53.86	50.76 (0.77)	48.70 – 53.86	49.31 (0.97)	46.39 – 51.83
ADF%	37.49 (7.27)	18.02 – 53.04	44.48 (4.53)	35.10 – 53.04	33.55 (5.29)	18.02 – 48.31
ADL%	21.95 (4.72)	8.27 – 36.76	26.16 (2.71)	20.22 – 8.27	19.58 (3.88)	8.27 – 30.34
Cellulose%	16.06 (2.69)	8.66 – 23.42	17.92 (2.33)	11.60 – 23.42	15.02 (2.29)	8.66 – 22.22
$\delta^{15}N‰$	-3.09 (1.68)	-7.98 – 0.41	-2.55 (1.97)	-7.75 – 0.41	-3.39 (1.41)	-7.98 – -0.53

979

980

981 **Table 2** Pearson product moment correlation coefficients between plot-level traits, latitude, mean annual precipitation (MAP), mean
982 annual temperature (MAT), latitude and NADP total annual N deposition (http://nadp.sws.uiuc.edu/).
983

	N%	M_{area}	C%	ADF%	ADL%	Cellulose%	$\delta^{15}N‰$	Lat	MAT	MAP
M_{area}	-0.766***									
C%	-0.618***	0.607***								
ADF%	-0.624***	0.700***	0.623***							
ADL%	-0.492***	0.649***	0.628***	0.931***						
Cellulose%	-0.476***	0.501***	0.386***	0.865***	0.746***					
$\delta^{15}N‰$	0.108	0.211**	0.005	-0.058	0.119	-0.226**				
Latitude	-0.312***	0.307***	0.106	0.170**	0.119	0.237**	-0.177**			
MAT	0.414***	-0.238**	-0.219**	-0.260***	-0.172**	-0.282***	0.413***	-0.862***		
MAP	-0.135*	-0.193**	0.203**	0.163**	0.087	0.088	-0.455***	-0.352***	-0.134*	
N Dep.	0.392***	-0.066	-0.278***	-0.165**	-0.121	-0.146*	0.398***	0.021	0.205**	-402***

984 $P < 0.0001$***; $P < 0.01$**; $P < 0.05$*
985
986
987
988

989 **Table 3** Summary of PLSR models built using AVIRIS spectra and foliar traits scaled to the plot level. Means of coefficients of
990 determination (R^2) and associated root mean squared error (RMSE) statistics of 500 randomized models are presented along with
991 associated uncertainty estimates (S.D. in parenthesis). Model-averaged fits indicate the accuracies obtained at the image level after
992 averaging predictions from 500 models.
993

	Traits		Model			Calibration		Validation		Model-averaged	
	Mean (S.D.)	Range	N	Train%	*h*	R^2	RMSE	R^2	RMSE	R^2	RMSE
M_{area}	107.28 (43.09)	51.88 – 224.53	202	28.82	10	0.92 (0.016)	12.68 (1.177)	0.81 (0.027)	18.20 (1.273)	0.88	15.039
N%	2.21 (0.56)	0.96 – 3.31	212	29.94	10	0.90 (0.019)	0.19 (0.016)	0.77 (0.028)	0.26 (0.015)	0.85	0.218
C%	49.68 (0.93)	46.94 – 51.73	208	29.47	10	0.67 (0.054)	0.55 (0.049)	0.44 (0.068)	0.69 (0.049)	0.63	0.568
ADF%	36.78 (7.10)	23.15 – 53.01	214	30.07	10	0.77 (0.041)	3.56 (0.317)	0.49 (0.062)	4.89 (0.299)	0.68	4.005
ADL%	20.99 (4.66)	10.53 – 30.57	211	29.50	12	0.86 (0.033)	1.80 (0.198)	0.52 (0.064)	3.16 (0.209)	0.74	2.343
Cellulose%	16.39 (2.50)	10.26 – 22.54	213	29.67	9	0.63 (0.059)	1.66 (0.151)	0.27 (0.062)	2.10 (0.104)	0.49	1.781
$\delta^{15}N$‰	-3.53 (1.33)	-6.90 – -0.74	190	28.30	8	0.59 (0.066)	0.89 (0.087)	0.29 (0.059)	1.14 (0.062)	0.48	0.954

994 Train%: Fraction of data used for model calibration; *h*: Number of components used to build PLSR models.
995

Figure Legends

Figure 1: Locations of field sampling plots (237) overlaid on AVIRIS acquisitions (143) from 2008-2011. Boxes indicate locations of sites graphed in subsequent figures; A: Porcupine Mountains SF, MI; B: Ottawa NF, MI; C Flambeau River SF, WI; D: Devil's Lake State Park, WI; E: Fernow Experimental Forest, WV; F: Green River SF, MD.

Figure 2: Scaling leaf-level functional traits to the canopy using AVIRIS imagery.

Figure 3: Means (with standard deviation bands) of AVIRIS spectra obtained from 51 images and 237 plots stratified by dominant leaf habit (deciduous, needleleaf).

Figure 4: PLSR model fits using AVIRIS-derived spectra fitted to foliar traits scaled from leaves to the canopy. Model performance evaluated by averaging 500 randomized models built with a 50/50 calibration/validation split. Horizontal bars indicate uncertainty in predictions; vertical bars indicate uncertainty in plot-level estimates propagated from leaf-level measurements, shading scheme of dots indicates increasing relative biomass of needleleaf foliage (white to black).

Figure 5: Standardized PLSR coefficients indicating the magnitude and direction of influence of each wavelength (with ±1 S.D. bands.) Note that raw coefficients are applied to image spectra to derive spatial predictions.Vertical dotted bars are absorption features at wavelengths known from

previous studies. Dashed gray lines indicate standardized coefficients from Serbin et al. (2014), white-filled line in %N subplot indicate coefficients from Martin et al. (2008).

Figure 6: Left column: Profile of the PRESS (predicted residual sum of squares) statistic (with ±1 S.D. bars) obtained by fitting 500 randomized models, each using an increasing number of PLS components (*h*, on the *x*-axis). The final model was fit using the components that minimized the PRESS statistic. Right column: Profile of the Variable Importance of Prediction (VIP) statistic with ±1 S.D. bands. The VIP describes the relative importance of each wavelength in predicting the quantity of interest, and is considered significant if > 0.8 (dotted line).

Figure 7: Spatial predictions of M_{area}, %N, %C, δ^{15}N‰, %Cellulose, %ADL and %ADF (left panels [means]; and uncertainties [standard deviations], right panels) obtained by applying 500 sets of coefficients obtained from randomized PLSR models to AVIRIS imagery acquired over the Green Ridge State forest, Maryland (box F, Fig. 1). Each model was built with a 50/50 calibration/validation split. See Table 3 for model statistics; supplement 2A for raw PLSR coefficients.

1037 **Figures**

1038 **Figure 1**

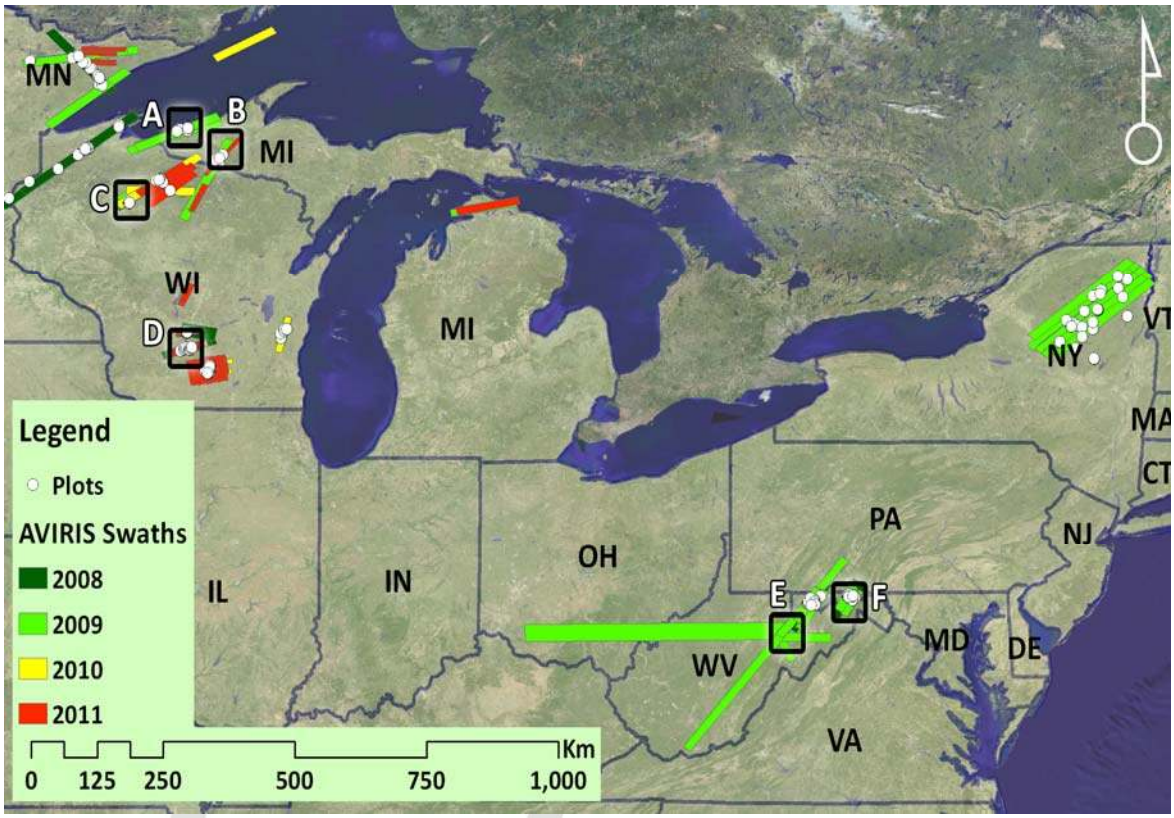

1039

1040

1041 **Figure 2**

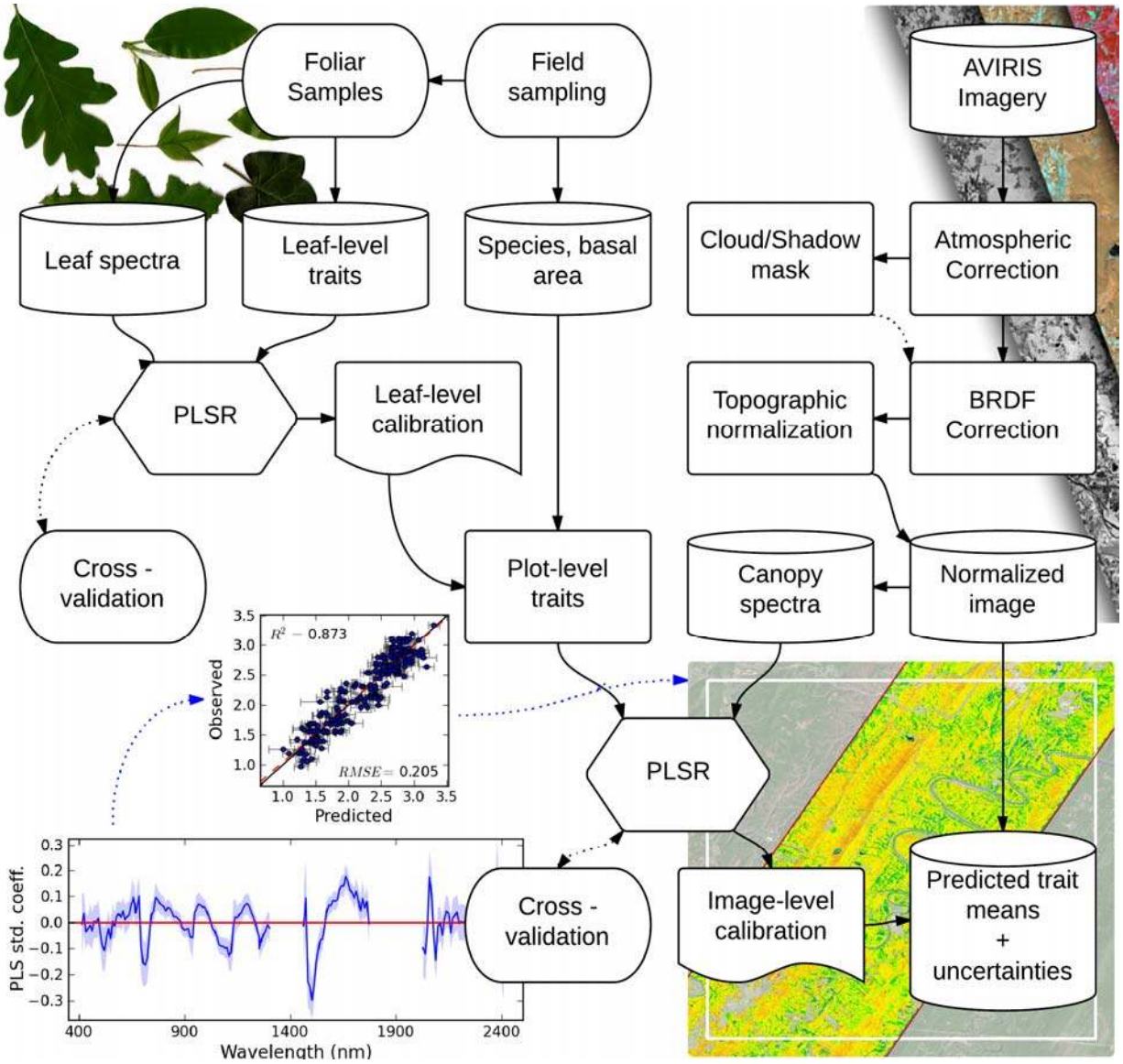

1042

1043

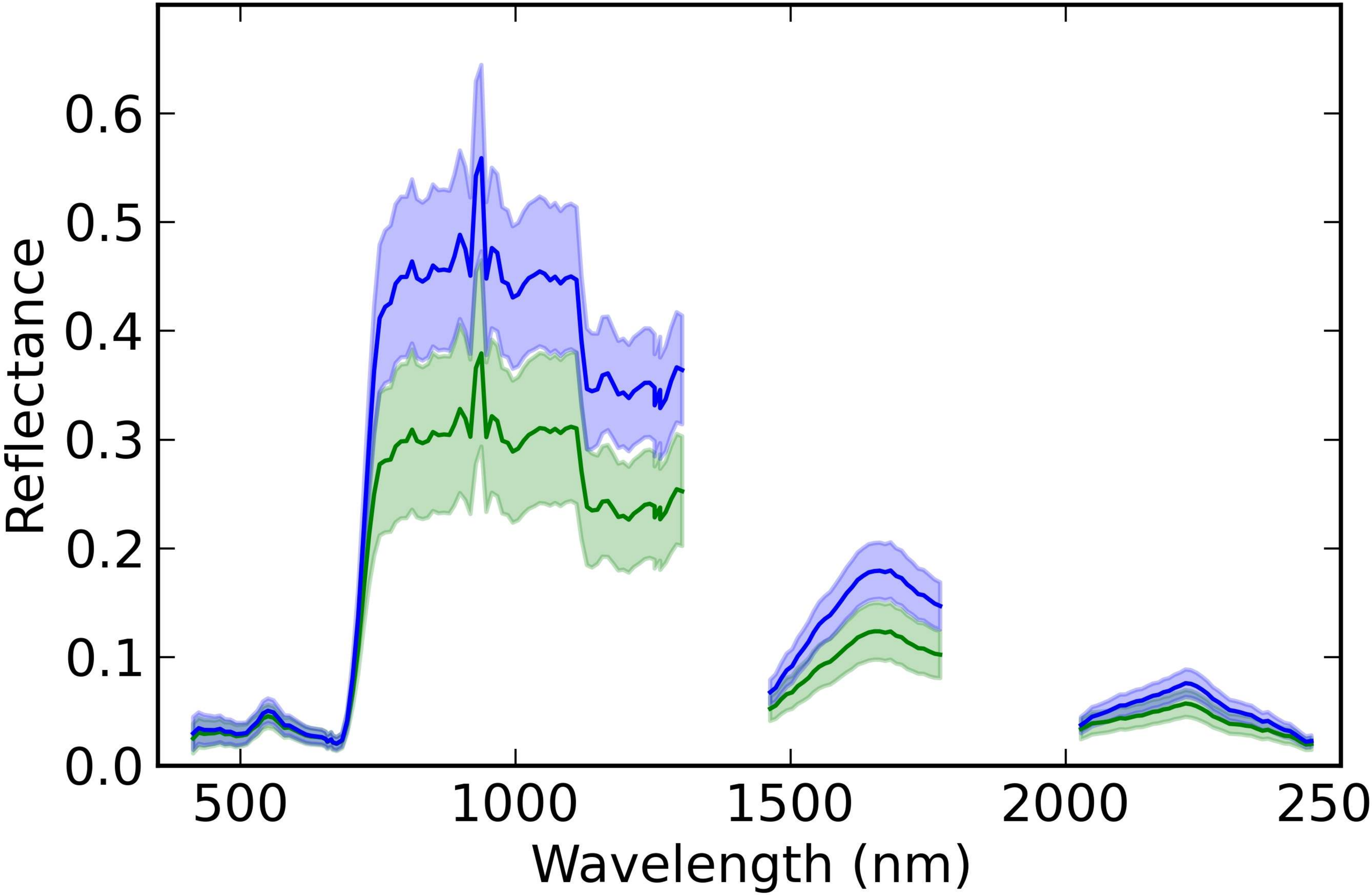
Reflectance
0.0
0.1
0.2
0.3
0.4
0.5
0.6
500
1000
1500
2000
250
Wavelength (nm)

%N

R^2 = **0.84**

$RMSE$ = **0.23**

M_{area}

R^2 = **0.88**

$RMSE$ = **15.06**

%C

R^2 = **0.65**

$RMSE$ = **0.57**

%ADF

R^2 = **0.70**

$RMSE$ = **3.72**

%ADL

R^2 = **0.76**

$RMSE$ = **2.17**

%Cellulose

R^2 = **0.47**

$RMSE$ = **1.68**

δN^{15} ‰

R^2 = **0.51**

$RMSE$ = **0.89**

Observed

Predicted

Predicted

% Needleleaf

0

25

50

75

100

%N
0.20
0.10
0.00
-0.10
-0.20
M_{area}
26.67
13.33
0.00
-13.33
-26.67
%C
1.00
0.50
0.00
-0.50
-1.00
PLS Standardized coefficient
%ADF
6.67
3.33
0.00
-3.33
-6.67
%ADL
5.33
2.67
0.00
-2.67
-5.33
%Cellulose
2.67
1.33
0.00
-1.33
-2.67
δN^{15} ‰
1.00
0.50
0.00
-0.50
-1.00
400
900
1400
1900
2400
Wavelength

Predicted residual sum of squares (PRESS)

PLS variable importance of prediction (VIP)

%N

M_{area}

%C

%ADF

%ADL

%Cellulose

δN^{15} ‰

PLS Components

Wavelength (nm)

Mean

S.D.

Mean

S.D.

M_{area} g/m²

400

20

30

5

Cellulose%

22

12

3.15

0.15

N%

3.5

1.0

0.45

0.05

ADL%

35

12

5.75

0.75

C%

52

48

1.25

0.15

ADF%

52

25

5.75

0.75

$\delta^{15}N‰$

-1.0

-6.0

2.5

0.25

Landcover

5 Km

Deciduous forest

Coniferous forest

Open water

Barren/Other